



Determination of the composition of human urinary calculi composed of whewellite, weddellite and carbonate apatite using artificial neural networks

Igor Kuzmanovski^{a,*}, Mira Trpkovska^a, Bojan Šoptrajanov^{a,b}, Viktor Stefov^a

^a *Institut za hemija, PMF, Univerzitet "Sv. Kiril i Metodij", P.O. Box 162, 1001 Skopje, Macedonia*

^b *Makedonska akademija na naukite i umetnostite, 1000 Skopje, Macedonia*

Received 19 December 2002; received in revised form 10 June 2003; accepted 20 June 2003

Abstract

More than half of the analyzed calculi from patients from Macedonia are composed of whewellite, weddellite and carbonate apatite (as single components or in binary or ternary mixtures). In order to develop a simple and satisfactorily reliable method for quantitative analysis of urinary calculi, the possibility was explored to employ artificial neural networks (ANNs) as a tool for such a purpose. By changing the number of input and hidden neurons, a search was made for the three-layered feed-forward ANN which would give the best performance. The root-mean-square errors (RMSE) for the test samples are: 0.035 for whewellite, 0.064 for weddellite and 0.078 for carbonate apatite. The accuracy of the method was checked using standard-addition method on real samples. The discrepancies between calculated and predicted mass fraction of constituents were in the range acceptable for use of the proposed method in clinical laboratories.

© 2003 Elsevier B.V. All rights reserved.

Keywords: Urinary calculi; Artificial neural network; Infrared spectroscopy; Whewellite; Weddellite; Carbonate apatite

1. Introduction

The development of automated methods for the determination of the composition of urinary calculi is very important since it can facilitate the determination of the factors which influence the occurrence of calculi in the urinary tract and perhaps aid the prevention of their reoccurrence. Among the instrumental techniques used for this purpose, the infrared spectroscopy is one of the most suitable ones [1]. Some of the main advantages of this technique are the simplicity of sam-

ple preparation and data collection, the specificity and reliability of the results and the small sample size that makes possible the study of the process of nucleation of the calculi. An additional advantage is the possibility to make a distinction between different hydrates (such as whewellite and weddellite) and to identify rarely appearing substances as constituents [2–5].

In the last 20 years, a number of computerized methods for the analysis of urinary calculi were developed [6–11]. Most of them are used for determining the qualitative and semi-quantitative composition using databases of infrared spectra of known constituents. Among the chemometric methods for quantitative determination of the composition human urinary calculi are the factor-based methods [12–14] as well as those which use the artificial neural networks

* Corresponding author. Tel.: +389-2-117-055;

fax: +389-2-226-865.

E-mail address: shigor@iunona.pmf.ukim.edu.mk

(I. Kuzmanovski).

(ANNs). In some of these methods [14,15], the accuracy of the method was determined by comparing the results with those obtained by visual inspection of a library of spectra. On the other hand, in [16] the standard-addition method was applied with the belief that the results thus obtained are more reliable and free from subjective errors. In fact, it is known [16–19] that the factor-based methods give best results when the relationship between absorbance and mass fraction of the analytes is close to linear, while the ANN methods are capable to model the non-linearities in the $A-w(B)$ relationships. The main advantages of ANNs over the traditional non-linear regression techniques is the fact that they are able to generate models without a priori knowledge about the modelling function [20]. Since ANNs and their application in chemistry have been extensively discussed in the chemistry literature [21,22], only the procedure applied for their optimization will be discussed here.

The recent statistical examination of the uroliths extracted from patients from Macedonia shows that about 54% of the analyzed calculi were composed of pure whewellite, pure weddellite or pure carbonate apatite or of binary and ternary mixtures of these substances [23]. In view of these findings, our goal was to develop a reliable method for quantitative analysis of such calculi, leaving the more complicated (and, as mentioned, less frequent) cases for further work.

2. Experimental

The infrared spectra of all samples (pure substances, prepared mixtures and real samples of urinary calculi) were recorded on a Perkin-Elmer System 2000 Fourier-transform infrared spectrophotometer in the $1450\text{--}450\text{ cm}^{-1}$ region with resolution of 4 and 1 cm^{-1} sampling interval. The samples were prepared as KBr pellets (2 mg of homogenized sample and 250 mg spectroscopy-grade KBr). If the maximum value of the absorbance in the recorded spectrum exceeded one, the mass of the sample in the pellet was proportionally reduced in order to achieve the desired maximum value of absorbance. The infrared spectra of the synthesized substances¹ (Fig. 1) were com-

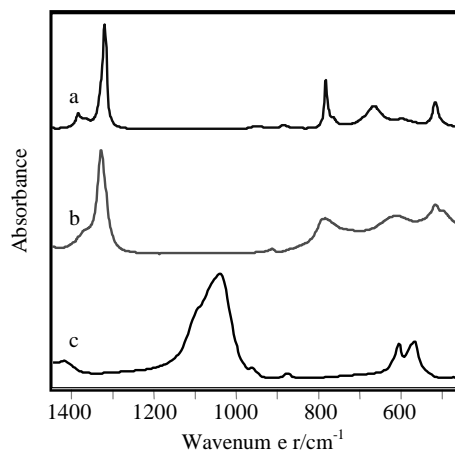


Fig. 1. Infrared spectra of (a) whewellite; (b) weddellite and (c) carbonate apatite in the $1450\text{--}450\text{ cm}^{-1}$ region.

pared with those in the digital database of infrared spectra by Dao and Daudon [27]. The comparison showed that the desired constituents have indeed been prepared and that the infrared spectra are of quality comparable to that in the database.

The optimization of the method was carried out on 58 samples prepared from synthetic whewellite, weddellite and carbonate apatite [21–23]. The mixtures used for the optimization of the method was prepared according to mixture design presented on Fig. 2.

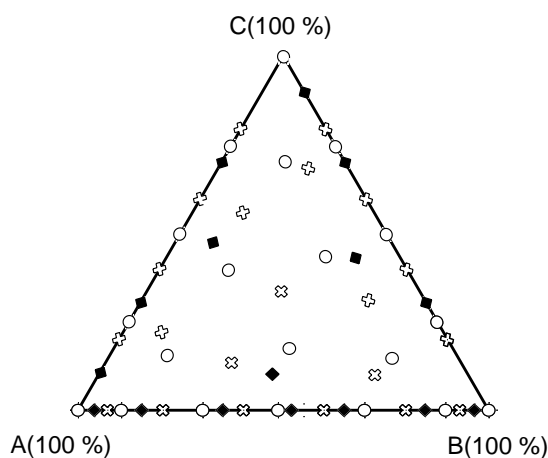


Fig. 2. Mixture design for the mixtures used for optimization of the neural networks: (A) whewellite; (B) weddellite; (C) carbonate apatite; (○) training set; (⊕) validation set; (◆) test set.

¹ The syntheses were carried out according to methods found in the literature [24–26].

Among the calculi consisting of whewellite, weddellite and carbonate apatite which were analyzed in our laboratory [23], those with mass of more than 100 mg were chosen. To each ground and homogenized sample, an exactly known mass (between 10.0 and 20.0 mg) of synthetic whewellite, weddellite and/or carbonate apatite was added. The infrared spectra of the samples were recorded before and after the standard addition.

2.1. Data analysis

All the recorded spectra were exported in ASCII format and stored in one data matrix. The rows in the data matrix corresponded to different samples, and each column to a different wavenumber value. The spectra in the data matrix were offset corrected (the minimum absorbance value in each spectrum was subtracted from the absorbance value at each wavenumber in the 1450–450 cm^{-1} region). The offset-corrected spectra were normalized to unit area. The data matrix of normalized spectra (\mathbf{D}) was used for further analysis. The mass fractions of the constituents of the prepared samples were stored in another data matrix in which each column corresponded to a given sample and each row to a different constituent. Another matrix (\mathbf{D}^m), consisting of mean-centered normalized spectra was also used in the course of the optimization. The elements of the latter matrix are defined as follows: $d_{i,j}^m = d_{i,j} - d_j$, where $d_{i,j}$ is element of \mathbf{D} , $d_{i,j}^m$ is the corresponding element of \mathbf{D}^m and d_j is the

average value of the absorbance at wavenumber j in \mathbf{D} .

A three-layered feed-forward neural network (Fig. 3) with a sigmoid transfer function in the hidden layer and a linear transfer function in the output layer was used. In order to improve the training rate and increase the performances of the ANN, an orthogonal transformation of the input variables (the absorbance values) was applied using the principal-component analysis [28].

The weights and biases of the networks were initialized according to Nguyen–Widrow algorithm. A training set was employed for weights and biases adjustment using the Levenberg–Marquardt algorithm [29] for back-propagation of error with the principal-components as input data and the mass fractions of constituents as target data.

The generalization abilities of the ANNs during the training process were monitored using a validation set, knowing that the validation error normally decreases during the training process. However, when the network begins to overtrain the data in the training set, the error in the validation set begins to increase. This finding could be used for controlling the generalization abilities of the optimized ANNs. The network training was stopped when the performance goal of 10^{-2} for the root-mean-square errors (RMSE) was reached or when in five consecutive iteration cycles the RMSE in the validation set increased. In the latter case, the weights and biases that correspond to the minimum validation error were restored.

The predictive power of the optimized networks was compared using the test set consisting of 17 prepared

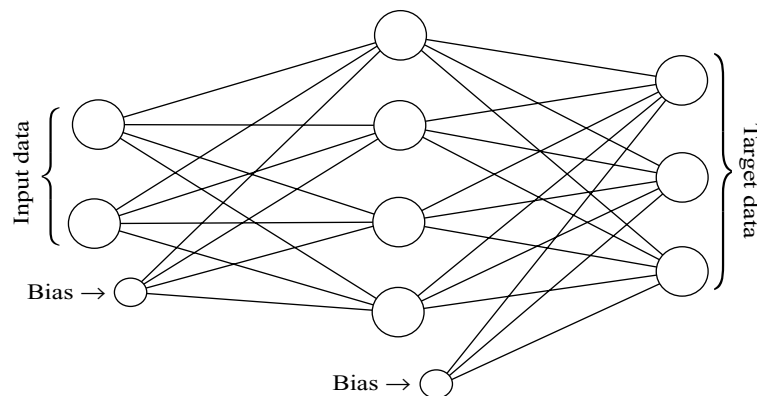


Fig. 3. Feed-forward artificial neural network with one input, one hidden and output layer.

mixtures (Fig. 2). The root-mean-square errors were used to estimate the prediction error:

$$\text{RMSE} = \left[\sum_{i=1}^m \sum_{j=1}^n \frac{(\bar{w}_{i,j} - w_{i,j})^2}{nm} \right]^{1/2} \quad (1)$$

where $\bar{w}_{i,j}$ is the predicted mass fraction of the constituent j in the i th sample, $w_{i,j}$ the calculated mass fraction of the constituent j the i th sample, m the number of the samples, and n the number of constituents in the samples in the test set.

The data processing was carried out using the MATLAB software package [30] and its Neural Network Toolbox [31].

3. Results and discussion

3.1. Neural network optimization

The process of finding the network architecture giving the best performances is a delicate and time-consuming task. The optimization of the ANNs presented in this work includes finding the optimal number of hidden and input neurons. The training of each network architecture was repeated 20 times in order to minimize the influence of the initial weights and biases on the performances of the optimized ANN.

3.2. Number of principal components

The data matrices consisting of normalized infrared spectra (\mathbf{D}) and of mean-centered normalized spectra (\mathbf{D}^m) were decomposed using the principal-component analysis. A total number of 1000 principal components (PCs) was calculated from both matrices. The auto-scaling (also known as standardization) is not recommended for the analysis of spectroscopic data since it unduly inflates the noise in baseline regions [32] and was not used in the present work.

The PCs which collectively carry 100.0% of the variance were used for optimization of different network architectures. In the case of the decomposition of \mathbf{D} , the first 12 PCs collectively capture 100.0% of the variance in the data. In the case of decomposition of \mathbf{D}^m , 100.0% of the variance was carried by 15 PCs.

Table 1

Percentage variance and cumulative percentage variance captured by each principal component

Number of PCs	Normalized data matrix		Normalized and mean centered data matrix	
	PV	CPV	PV	CPV
1	86.19	86.19	67.82	67.82
2	7.18	93.37	25.48	93.30
3	4.45	97.82	4.48	97.78
4	2.06	99.88	1.40	99.18
5	0.04	99.92	0.38	99.56
6	0.03	99.95	0.20	99.76
7	0.02	99.97	0.11	99.86
8	0.01	99.98	0.05	99.92
9	0.00	99.99	0.03	99.95
10	0.00	99.99	0.02	99.97
11	0.00	99.99	0.01	99.98
12	0.00	100.00	0.01	99.99
13	0.00	100.00	0.00	99.99
14	0.00	100.00	0.00	99.99
15	0.00	100.00	0.00	100.00

The percentage variance (PV) as well as the cumulative percentage variance (CPV) captured by these PCs are presented in Table 1.

It could be noticed that in both cases (\mathbf{D} and \mathbf{D}^m) most of the variance (more than 93% of the cumulative variance) is captured by the first two PCs. This is probably so because when using spectra normalized to unit area of a three-component mixture (and where, as in our case, the compositions of the mixtures is expressed using mass fraction), only two parts of the normalized area are independent, while the part of the area which corresponds to the third component will always have to complement the area to unity.

The mean values² of the calculated RMSE for the test set as a function of the number of input neurons is presented in Fig. 4. This figure shows that the average performance of the ANNs increase (the RMSE values sharply decrease) as the number of input neurons increases, and reach a minimum RMSE when (in the case of \mathbf{D} and \mathbf{D}^m data matrices) three PCs were used as input data. However, after the minimum for RMSE is reached, the average network performance starts to decrease.

² Calculated from all network architectures (different number of neurons in the hidden layer) and from RMSE values obtained by 20 repetitions of the training of the different network architectures.

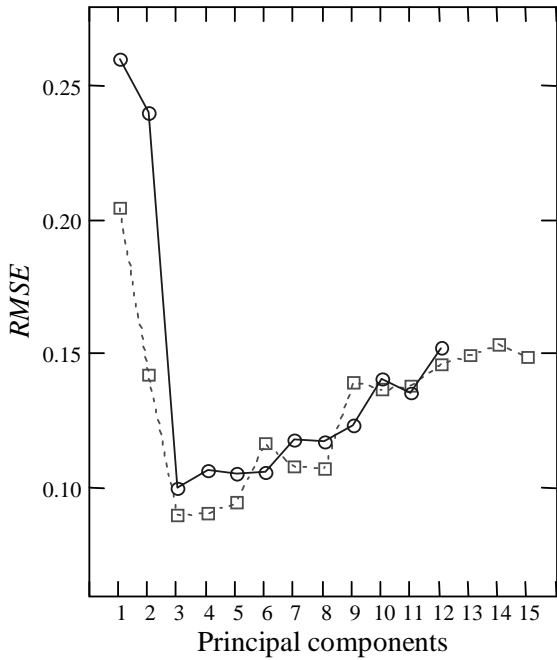


Fig. 4. Mean RMSE as a function of the number of principal components obtained from normalized (○) and normalized and mean-centered data matrix (□).

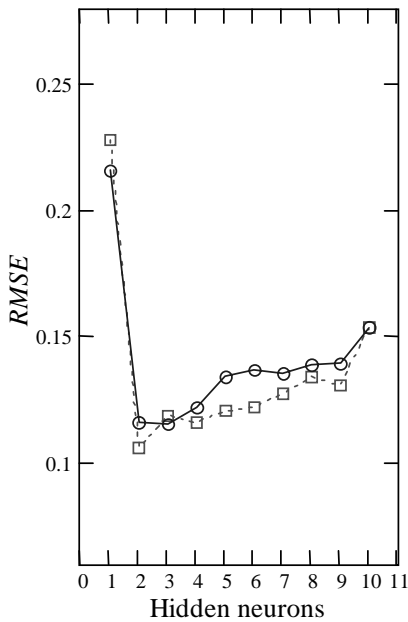
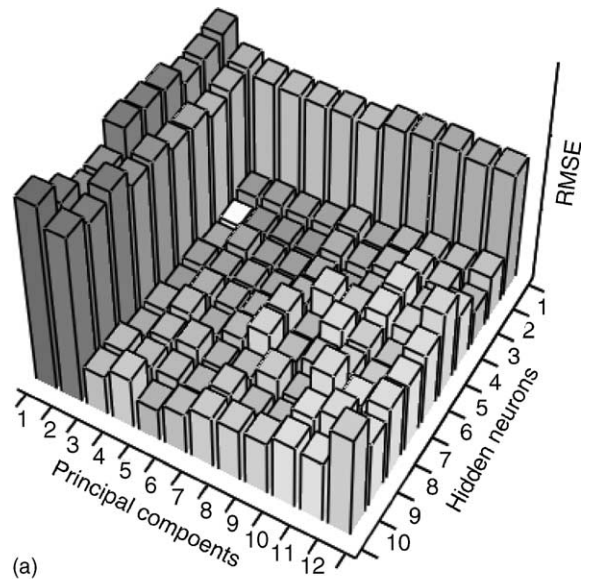


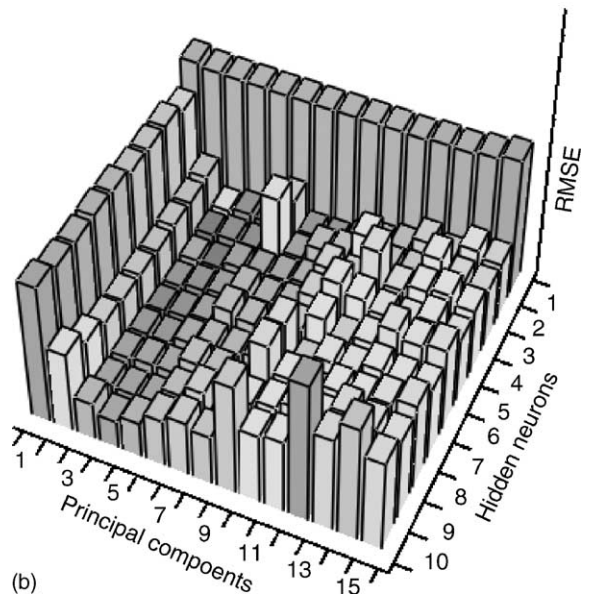
Fig. 5. Mean RMSE as a function of the number of hidden neurons for normalized (○) and normalized and mean-centered data matrix (□).

3.3. Number of hidden neurons

The number of neurons in hidden layer defines the complexity of the developed model. If the number of neurons in the hidden layer is too small, the ANN will



(a)



(b)

Fig. 6. Mean RMSE for all network architectures (obtained by: (a) normalized data matrix and (b) normalized and mean-centered data matrix).

Table 2
Calculated and predicted mass fractions for the component of some of the analyzed calculi using ANN with best performances

Sample	Calculated mass fraction of constituents after standard addition			Predicted mass fraction of constituents after standard addition			Difference between calculated and predicted mass fractions of the samples after standard addition			Standard deviations for the predicted mass fraction of constituents after standard addition		
	Whewellite	Weddellite	Carbonate apatite	Whewellite	Weddellite	Carbonate apatite	Whewellite	Weddellite	Carbonate apatite	Whewellite	Weddellite	Carbonate apatite
1	0.293	0.339	0.368	0.301	0.317	0.382	-0.008	0.022	-0.014	0.050	0.029	0.046
2	0.307	0.537	0.155	0.320	0.559	0.121	-0.012	-0.022	0.034	0.021	0.016	0.017
3	0.301	0.436	0.263	0.264	0.358	0.378	0.037	0.078	-0.115	0.057	0.036	0.051
4	0.321	0.257	0.421	0.316	0.258	0.425	0.005	-0.001	-0.004	0.065	0.036	0.057
5	0.033	0.650	0.317	0.064	0.510	0.427	-0.031	0.140	-0.109	0.072	0.052	0.072
6	0.368	0.347	0.285	0.342	0.307	0.351	0.026	0.040	-0.066	0.034	0.019	0.035
7	0.331	0.365	0.305	0.339	0.364	0.297	-0.008	0.001	0.007	0.059	0.039	0.050
8	0.316	0.536	0.148	0.312	0.513	0.175	0.005	0.022	-0.027	0.056	0.042	0.040
9	0.310	0.451	0.239	0.261	0.455	0.284	0.049	-0.004	-0.045	0.022	0.019	0.027

not be able to model the data accurately. If, on the other hand, the number of neurons in hidden layer is too large, the performances of the ANN will deteriorate [33]. The influence of the number of hidden neurons on network performances of different networks architectures is presented on Fig. 5. It shows that the mean values of RMSE in the beginning decreases and after reaching a minimum (at three hidden neurons for ANNs where PCs were obtained from data matrix of normalized spectra and two hidden neurons for ANNs trained with PCs calculated from the mean centered data matrix) begins to increase slightly. In Fig. 5 also the average performances for network architectures as a function of the number of hidden neurons also shows that ANNs trained with PCs calculated from mean centered data matrix have the best average performances.

The comparison of the performances of all the network architectures is presented in Fig. 6. The network architectures giving the best average performances for both data matrices used for PCA were found. When the ANNs were trained with PCs calculated from normalized data matrix, the network giving the best performances is that with three input and three hidden neurons. The average RMSE of this network is 0.070 and it is slightly better than the one obtained by the best network architecture (which has three input neurons and two hidden neurons) found when mean centered data were used (RMSE = 0.073).

The same trends on RMSE as a function of number of hidden neurons and principal components used for optimization, could be observed in the case of the network architectures trained by PCs calculated from *D*. Here, it was found that the network with best average performances is that trained using three PCs and with three neurons in the hidden layer. The calculated RMSE for the constituents of the test set are: 0.035 for whewellite, 0.064 for weddellite and 0.078 for carbonate apatite.

3.4. Analysis of real samples

The network giving the best performances (the one with three input neurons and three hidden neurons) was applied for predicting the composition of urinary calculi consisted of whewellite, weddellite and carbonate apatite. The accuracy of the obtained results was checked using the method of standard additions—adding an exactly known mass of synthetic whewellite,

weddellite or carbonate apatite to an exactly known mass of the carefully ground and homogenized calculus.

The mass fractions of the constituents in the samples before and after standard addition were determined by the same ANN. Knowing the predicted composition of the samples without standard additions, the mass of the samples used for standard addition as well as the mass of the added standard, the expected mass fractions were calculated. The calculated mass fractions of the constituents with standard addition, the predicted mass fractions for the samples with standard addition and the standard deviations for each of the constituents of the analyzed samples are present in Table 2. In most cases the absolute values of the differences between the predicted and the calculated mass fraction of the constituents of the samples are smaller than 0.10. The standard deviations of the predicted mass fractions of the constituents vary from 0.016 up to 0.072 in the case of sample number 5 where the bigger discrepancies between predicted and calculated mass fractions are observed, while according to the data presented in the literature, the methods where standard deviations, varies between 0.050 and 0.100 are suitable for determining the composition of urolithes in clinical laboratories [34].

4. Conclusion

The quantitative composition of urinary calculi composed of whewellite, weddellite and carbonate apatite was determined using a feed-forward ANN. In order to make the training procedure faster and to get better results, the principal-component analysis was applied on normalized spectra. The PCs were used as input parameters for training the feed-forward networks. The influence of the number of input neurons (principal components) and number of hidden neurons on the network performances was investigated. This work shows that networks trained with three input and three hidden neurons are capable of prediction of the constituents in the urinary calculi composed of whewellite, weddellite and carbonate apatite with best average performances. This network architecture was used for prediction of the real samples of urinary calculi composed of the whewellite, weddellite and carbonate apatite.

The absolute values of the differences between predicted and calculated mass fractions of the constituents (in most of the cases <0.10) as well as their standard deviations (varying from 0.016 up to 0.072) shows, that this method is suitable for prediction of the composition of this type of urinary calculi [34].

The procedure described here is consisted of many steps of data treatment (exporting the spectra in ASCII format, normalization of the spectra, principal-component analysis, optimization of the network and prediction of the mass fractions of the constituents using trained network), which could make this method complicated for routine use in clinical laboratories, but the procedure described here could be relatively easy automated if specialized software is developed. This will “hide” the data treatment under the suitable graphical user interface, which will make the method simpler for use in clinical laboratories.

References

- [1] M. Daudon, R.J. Reveillaud, *Presse. Med.* 16 (1987) 627–631.
- [2] D. Beischer, *J. Urol.* 73 (1955) 653.
- [3] K. Try, *Scand. J. Urol. Nephrol.* 15 (1981) 263.
- [4] M. Daudon, M.F. Protat, R.J. Reveillaud, *Ann. Biol. Clin.* 36 (1978) 475.
- [5] K. Stojanova, I. Petrov, B. Šoptrajanov, *Maked. Med. Pregled* 24 (1969) 71.
- [6] S.H. Kandil, T.A. Abou El Azm, A.M. Gad, M.M. Abdou, *Comput. Enhanced. Spectrosc.* 3 (1986) 171.
- [7] M. Berthelot, G. Cornu, M. Daudon, M. Helbert, C. Laurence, *Clin. Chem.* 33 (1987) 2070.
- [8] C.A. Lehmann, G.L. McClure, I. Smolens, *Clin. Chim. Acta* 173 (1988) 107.
- [9] A. Hesse, M. Gergeleit, P. Schüller, K. Möller, *J. Clin. Chem. Clin. Biochem.* 27 (1989) 639.
- [10] G. Rebentisch, M. Doll, J. Mucbe, *Lab. Med.* 16 (1992) 224.
- [11] E. Peuchant, X. Heches, D. Sess, M. Clerc, *Clin. Chim. Acta* 205 (1992) 19.
- [12] I. Kuzmanovski, M. Trpkovska, B. Šoptrajanov, V. Stefov, *Vib. Spectrosc.* 19 (1999) 249.
- [13] H. Hobert, K. Meyer, *Fresenius' J. Anal. Chem.* 334 (1992) 178.
- [14] M. Volmer, A. Block, B.G. Wolthers, A.J. de Ruiter, D.A. Doornbos, W. van der Slik, *Clin. Chem.* 39 (1993) 948.
- [15] M. Volmer, A. Block, H.J. Metting, T.H.Y. de Haan, P.M.J. Coenegracht, W. van der Slik, *Clin. Chem.* 40 (1994) 1692.
- [16] I. Kuzmanovski, M. Trpkovska, B. Šoptrajanov, V. Stefov, *Fresenius' J. Anal. Chem.* 370 (2001) 919.
- [17] C. Borggaard, H.H. Thodberg, *Anal. Chem.* 64 (1992) 545.
- [18] E.V. Thomas, D.M. Haaland, *Anal. Chem.* 62 (1990) 1091.
- [19] K.R. Beebe, B.R. Kowalski, *Anal. Chem.* 59 (1987) 1007A.
- [20] A.R. Barron, *IEEE Trans. Inform. Theory* 39 (1993) 930.
- [21] J. Zupan, J. Gasteiger, *Neural Networks in Chemistry and Drug Design*, Wiley, New York, 1999.
- [22] A. Bos, M. Bos, W.E. van der Linden, *Anal. Chem. Acta* 256 (1992) 133.
- [23] I. Kuzmanovski, M. Trpkovska, B. Šoptrajanov, *Maked. Med. Pregled* 53 (1999) 251.
- [24] P. Brown, D. Ackermann, B. Finlayson, *J. Cryst. Growth* 98 (1989) 285–292.
- [25] D. Ackermann, P. Brown, B. Finlayson, *Urol. Res.* 16 (1988) 219–220.
- [26] M. Santos, P.F. González-Díaz, *Inorg. Chem.* 16 (1977) 2131.
- [27] N.Q. Dao, M. Daudon, *Infrared and Raman Spectra of Calculi*, Elsevier, Paris, 1997.
- [28] P.J. Gemperline, J.R. Long, V.G. Gregoriou, *Anal. Chem.* 63 (1991) 2313.
- [29] M.T. Hagan, M. Menhaj, *IEEE Transactions on Neural Networks*, 1994, p. 989.
- [30] *MATLAB 5.2, 1984–1998 Mathworks.*
- [31] H. Demuth, M. Beale, *Neural Network Toolbox*, Mathworks, Natick, 1997.
- [32] R. De Maesschalck, F. Estienne, J. Verdú-Andrés, A. Candolfi, V. Centner, F. Despagne, D. Jouan-Rimbaud, B. Walczak, D.L. Massart, S. de Jong, O.E. de Noord, C. Puel, B.M.G. Vandeginste, *Int. J. Chem.* 2 (1999) 1.
- [33] F. Despagne, D.L. Massart, *The Analyst* 123 (1998) 157R–178R.
- [34] A. Hesse, G. Sanders, R. Döring, J. Oelichmann, *Fresenius' J. Anal. Chem.* 330 (1988) 372.